LAWRENCE
LIVERMORE
NATIONAL
LABORATORY

LLNL-CONF-554011

Modeling Responses of Naturally Fractured Geothermal Reservoir to Low-Pressure Stimulation

P. Fu, C. R. Carrigan

May 1, 2012

36th Annual Meeting of the Geothermal Resources Council
Reno, NV, United States
September 30, 2012 through October 3, 2012

Disclaimer

Modeling Responses of Naturally Fractured Geothermal Reservoir to Low-Pressure Stimulation

Pengcheng Fu, Charles R. Carrigan
Atmospheric, Earth, and Energy Division, Lawrence Livermore National Laboratory
7000 East Ave., L-286
Livermore, CA 94550, USA
e-mail: fu4@llnl.gov

Abstract:

Hydraulic shearing is an appealing reservoir stimulation strategy for Enhanced Geothermal Systems. It is believed that hydro-shearing is likely to simulate a fracture network that covers a relatively large volume of the reservoir whereas hydro-fracturing tends to create a small number of fractures. In this paper, we examine the geomechanical and hydraulic behaviors of natural fracture systems subjected to hydro-shearing stimulation and develop a coupled numerical model within the framework of discrete fracture network modeling. We found that in the low pressure hydro-shearing regime, the coupling between the fluid phase and the rock solid phase is relatively simple, and the numerical model can achieve a low computational cost. Using this modified model, we study the behaviors of a random fracture network subjected to hydro-shearing stimulation.

Keywords: hydraulic fracturing; hydraulic shearing; reservoir stimulation; reservoir modeling; discrete fracture network

1. Introduction

A tremendous amount of geothermal energy exists at depths within the accessible range of routine drilling technologies (MIT, 2006). However, the extremely low natural permeability in these geologic formations prevents effective and economical extraction of heat. Various reservoir stimulation methods, especially hydraulic stimulation techniques can be used to enhance the permeability in rocks and have been successfully applied in other sectors such as shale gas development. The primary form of hydraulic stimulation is hydraulic fracturing, which aims at creating new fractures by pumping fluid at pressure higher than the minimum *in situ* principal stress in the rock. However, concerns have been raised regarding the tendency of hydraulic fracturing to create a single or a small number of hydraulic fractures if applied in Enhanced Geothermal Systems (EGS, also termed Engineered Geothermal Systems). Even though it is possible to achieve high permeability in such a stimulated reservoir between the injection well and the production well if they are connected by propped fractures, only the heat in a small vicinity of these fractures can be effectively extracted.

An alternative stimulation strategy is to stimulate naturally fractured reservoirs with pressure slightly lower than the *in situ* compressive stress. This method works for reservoirs with natural fractures that are already inter-connected. These fractures are all tightly closed under the high subsurface pressure, so the natural permeability of the unstimulated rock body is very low. The low-pressure fluid, although not able to create a substantial amount of new fractures or completely "open" existing fractures, can significantly reduce the effective normal stress on existing fractures. Because *in situ* shear stress more or less exists

along the natural fractures, shear slipping and the associated shear dilation can take place if the effective normal stress is sufficiently low. The permeability improvement caused by shear dilation persists even after the stimulation pressure decreases and effective normal stress resumes after the stimulation, resulting in permanent permeability enhancement. This process is termed "hydraulic shearing" or "hydro-shearing" to be differentiated from the more commonly used process of hydraulic fracturing. Note that a fracture is considered "open" if the two walls along this fracture have been completely separated by pressurized fluid between them. On the other hand, the two walls of a "partially open" fracture are still in contact and fluid pressure and contact stress bear the total normal stress together.

A small number of models are available for simulating hydro-shearing (Willis-Richards et al., 1996; Jing et al., 2000; Rahman et al. 2002; Tezuka et al., 2005; Cladouhos et al. 2011). Due to the inherent complexity in this process, many simplification assumptions had to be made to make the numerical problem tractable, some of which are not necessarily appropriate. In this paper, we examine the mechanical behavior of rock-fracture-fluid systems experiencing hydro-shearing, identify key physical processes that need to be simulated in the model, and thereby formulate a discrete fracture network (DFN) –based model for studying the effectiveness of hydro-shearing in stimulating geothermal reservoirs.

2. Formulation of the numerical model

2.1 Response of pressurized fracture in normal direction

Closed fractures, including partly open fractures under pressure are considered "joints" in rock mechanics. The closure behavior of a fracture, namely the variation of the effective aperture width w with respect to the effective stress σ' is characterized by the following model (Bandis et al., 1983; Barton et al. 1985)

$$\sigma' = \frac{w_{max} - w}{a - b(w_{max} - w)} \qquad (1)$$

where w_{max} is the aperture width at the zero-effective stress state, which is essentially the *maximum joint closure* in the original joint model of Bandis et al.; a and b are two material- and state-specific constants. If we identify an second reference state with effective normal stress σ'_{ref} and aperture width w_{ref}, the two material can be calculated as

$$a = w_{max}\frac{w_{max} - w_{ref}}{\sigma_{ref} w_{ref}} \text{ and } b = \frac{w_{max} - w_{ref}}{\sigma_{ref} w_{ref}} \qquad (2)$$

This closure model is used here to characterize the variation of aperture width as a function of fluid pressure inside the fracture.

2.2 Consideration of back stress

When a fracture dilates as it is pressurized by fluid or shear slipping takes place, it generates additional stress in the surrounding rock matrix, which is termed the "back stress". If the fracture is only partly open, the change of back stress can be approximately estimated using the following equation

$$\Delta\sigma_M \approx \frac{\Delta w}{\tilde{L}} E' \qquad (3)$$

where $\Delta\sigma_M$ is the increment of rock matrix stress normal to the fracture due to fracture dilation, i.e. the back stress increment; Δw is the aperture width change; E' is the confined stiffness of the rock matrix and can be approximately by the Young's modulus; and $\widetilde{L}$ is a characteristic length scale that quantifies the kinematic constraints surrounding the fracture. $\widetilde{L}$ is related to the distance from the current fracture to parallel fractures that are also pressurized or other kinematic constraints, and also related to the length of the fracture. We assume that Δw is a small fraction of a millimeter, E' is tens of GPa, and $\widetilde{L}$ is a few meters based on general rock mechanics knowledge. Consequently, $\Delta\sigma_M$ is generally no more than a couple MPa, significantly smaller than the typical magnitude of *in situ* stress at the depth of EGS applications. Note that Δw is bounded by w_{max} and $\widetilde{L}$ is related to the fracture density in the rock matrix. This finding implies that the stress shadowing effect induced by the back stress, namely the dilation of neighboring fractures increasing the total normal stress of each other, is insignificant for partly open fractures in the hydraulic shearing regime. On the other hand, if the fluid pressure exceeds the original normal stress of the fracture and the fracture opens completely, the rock matrix stress increment must balance the fluid pressure increment, so the stress shadowing effect will be very significant, which belongs to a fundamentally different regime.

2.3 Discrete fracture flow solver

The discrete fracture flow solver in this model is modified based on the flow solver in Fu et al. (2011). In the original solver developed for hydro-fracturing applications, the aperture width of open fractures is determined by the rock matrix deformation calculated in the finite element solid solver. For hydro-shearing applications, the aperture width can be simply calculated according to equation (1) if we ignore the interactions between neighboring pressurized fractures through the stress shadowing effect.

Fluid flow in partly open rock fractures is idealized as laminar flow between two parallel plates employing lubrication theory. The governing equations are

$$\frac{\partial q}{\partial l}+\frac{\partial w}{\partial t}=0 \tag{4}$$

$$\frac{(w^h)^3}{12\mu_F}\frac{\partial P_F}{\partial l}=-q \tag{5}$$

$$\sigma_M - P_F = \frac{w_{max}-w}{a-b(w_{max}-w)} \tag{6}$$

where l represents the length along the fracture; q is the local flow rate in the fracture at a given cross-section; w is the local time- and pressure-dependent aperture width; P_F is the local fluid pressure; μ_F is the dynamic viscosity the fluid; σ_M is the total normal stress applied on the fracture. Equation (4) is the continuity (mass conservation) equation; equation (5) is the permeability equation, according to the laminar parallel plate flow assumption. These governing equations are solved with a two-dimensional finite volume method (FVM) based in an explicit time integration scheme, as described in Fu et al. (2011).

In every time step, the flow solver loops through all the flow nodes and calculates the flow rate of each cell from and to its two nodes, thereby obtaining the mass increment and updated fluid mass in the cell. The average fluid pressure in each cell is related to the fluid density through the following equation-of-state (EOS)

$$P_F = \begin{cases} K_F\left(1-\dfrac{\rho_{ref}L_C w}{m_C}\right) & \text{if } m_C / L_C w \geq \rho_{ref} \\ P_{vap} & \text{if } m_C / L_C w < \rho_{ref} \end{cases} \qquad (7)$$

where K_F is the bulk modulus of the fluid; ρ_{ref} is the reference density of this fluid, namely the density at zero or the datum pressure; L_C is the length of the fluid cell and w is the aperture width, so $L_C w$ is the fluid storage volume of the cell; m_C is the updated fluid mass in this cell; P_{vap} is the temperature-dependent vapor pressure of this fluid which can be considered to be zero for the purpose of hydraulic stimulation modeling as the pumping pressure is many orders of magnitude higher than the vapor pressure.

We plug the upper branch of equation (7) into equation (6) to convert the EOS of the fluid into the EOS of the fracture

$$\sigma_M - K_F\left(1-\frac{\rho_{ref}L_C w}{m_C}\right) = \frac{w_{max}-w}{a-b(w_{max}-w)} \qquad (8)$$

which can be solved as

$$w = w_{max} - \frac{Aa+Bb+1-[(Aa+Bb+1)^2-4AaBb]^{0.5}}{2Ab} \qquad (9)$$

where $A=K_F\rho_{ref}L_C/m_C$ and $B=\sigma_M-K_F+Aw_{max}$ are two constants to simplify the expression of the equations. With this equation, we can directly calculate the aperture width at each time step from the updated fluid mass and then obtain the fluid pressure using equation (7). The updated aperture width and pressure distribution is used in the next time step for the calculating of flow rate.

2.4 Modeling shear-induced self-propping

The potential effectiveness of hydro-shearing stimulation is rooted in the assumption that shear dilation takes place and results in permanent permeability enhancement under the following conditions: 1) There exists significant shear stress long the fractures; and 2) the fluid pressure is sufficiently high to induce shear slipping of the fractures as a result of the reduced effective stress. Predicting the amount of shear dilation is a challenging task, primarily due to the lack of experiment data that enable characterization of joint behaviors along the complex stress paths associated with hydraulic stimulation and the subsequent drawdown after stimulation. The following simple phenomenological empirical model is used in this study to represent the most important shear dilation behaviors associated with low pressure stimulation.

A variable termed the stimulation factor S is introduced to quantify the extent to which a fracture has been stimulated through shear dilation. With S incorporated in the formulation, the joint closure curve (σ'-w curve) is dependent on this state variable. Note that S is a state variable of each flow cell (a small segment of a fracture) in the discretized finite volume model instead of being a parameter for the whole fracture network. The three parameters in equation (1), w_{max}, a, and b are functions of S. If we assume the effects of σ' and those of S in determining the aperture width can be decoupled, S becomes a multiplier of the original joint model as

$$w = w(\sigma', S) = Sw(\sigma') \qquad (10)$$

In the unstimulated state, $S=S_0=1$.We denote the three parameters in the joint model in this state as w_{max0}, a_0 and b_0, and the evolution of these parameters with S is as $w_{max} = w_{max0}S$ and $a = a_0S$ while b happens to be a constant as $b=b_0$. We define the "excessive" shear stress along a fracture to be $\tau'=\max(\tau_0-\sigma'\mu_J, 0)$, where τ_0 is the shear stress along the fracture in the initial state without hydraulic pressure and μ_J is coefficient of friction of the fracture. The stimulation factor S is assumed to be related to the greatest excessive shear stress τ'_{max} ever achieved by the fracture

$$S = \begin{cases} 1+\tau'_{max}(S_{max}-1)/\tau'_s & \text{if } \tau'_{max} < \tau'_s \\ S_{max} & \text{otherwise} \end{cases} \qquad (11)$$

where S_{max} is the upper limit of S and S reaches S_{max} at excessive shear stress τ'_s. The above formulation dictates that an increase of the excessive shear stress can induce increase of S, but a decrease of τ' has no effect on S. In other words, the stimulation effects induced by the increase of fluid pressure will not be reversed when the pressure decreases after the stimulation. However, the aperture size is still a function of the effective stress as dictated by equation (8). The main effect of stimulation by shear dilation is to change the values of the constants in equation (1).

An example shown in Figure 1 illustrates the evolution of the state of a joint element during hydraulic shearing. In the initial state before pressurized fluid is pumped into this fracture, the normal effective stress and the corresponding aperture width is represented by point O in the figure. As the fluid pressure increases and the normal effective stress decreases, the σ'-w state evolves along the original σ'-w curve until state A is reached, where shear slipping and the associated shear dilation take place. Along path 0-A, the stimulation factor S remains unchanged. As σ' further decreases beyond point A, S will evolves according to the rule defined by equation (11). For instance, states B and C are associated with different S values. If we reduce the fluid pressure at point B, the σ'-w relationship will follow the closure curve through point B.

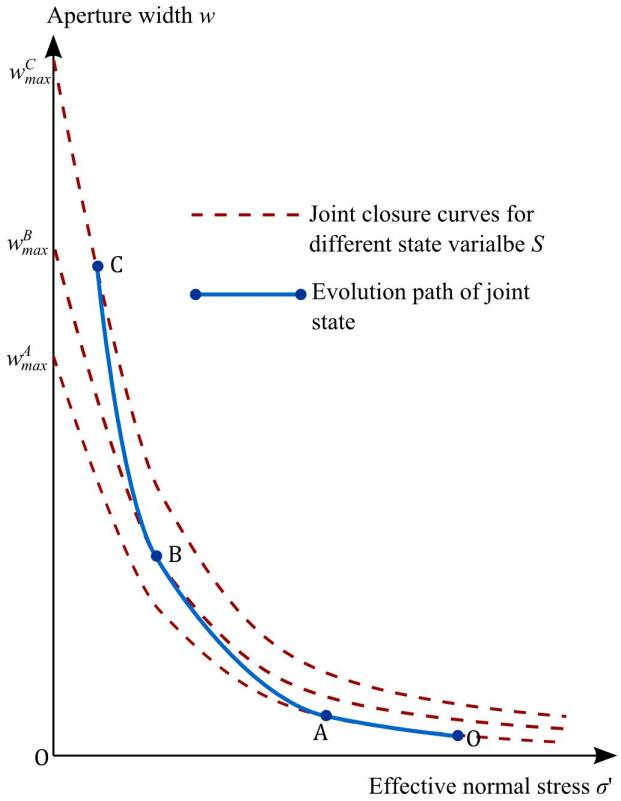

Figure 1 The evolution of fracture state (σ'-w) during hydro-shearing.

Numerical example

In this section, we investigate the responses of a virtual reservoir to different hydro-shearing stimulation scenarios using the numerical model developed. As shown in Figure 2, the simulation domain extends from -160 m to 160 m in the x-direction and from 0 to 240 m in the y-direction. There are two sets of joints (existing natural fractures) in this reservoir. The horizontal set has orientation angles (rotating counterclockwise from the x-axis) with a uniform distribution between 10° and 30° whereas the vertical set has orientation angles between 80° and 100°. This 2D simulation domain should be considered as a plan view of the reservoir, so the term "vertical" refers to the direction within the image, not the vertical direction in a 3D space. All the fractures have lengths between 20 m and 60 m and the total length of fractures in the two sets are 8,300 m and 8,700 m, respectively. The discrete fracture system is discretized into finite volume cells with an average length of 1.0m. The injection well is located near the middle point of the lower boundary of the domain as shown in Figure 4, so the simulation is on a half of the reservoir. The location of the production well is shown in Figure 4. The far field *in situ* stress applied is σ_{xx}=-20 MPa, σ_{yy}=-28 MPa, and σ_{xy}=2 MPa, following signing conventions in solid mechanics (i.e. tension is positive). The minimum compressive principal stress direction is 13° rotating counterclockwise from the x-axis. The normal and shear *in situ* stresses on an average horizontal fracture (20° from the horizontal) are 28.3 MPa and 1.0 MPa, respectively. The normal and shear *in situ* stresses on an average vertical fracture (90° from the horizontal) are 19.7 MPa and 1.0 MPa, respectively. Since most of the fractures do not exactly align with the principal stress directions, shear stress dependent on the orientation angle of fractures. Important model parameters used is this study are summarized in Table 1.

Table 1: Model parameters used in this study.

Parameter	Value
w_{max0}	0.5 mm
w_{ref0}	0.05 mm
σ_{ref}	20 MPa
τ'_s	4 MPa
S_{max}	3.0
μ_J	0.7
μ_F	0.001 Pa·s

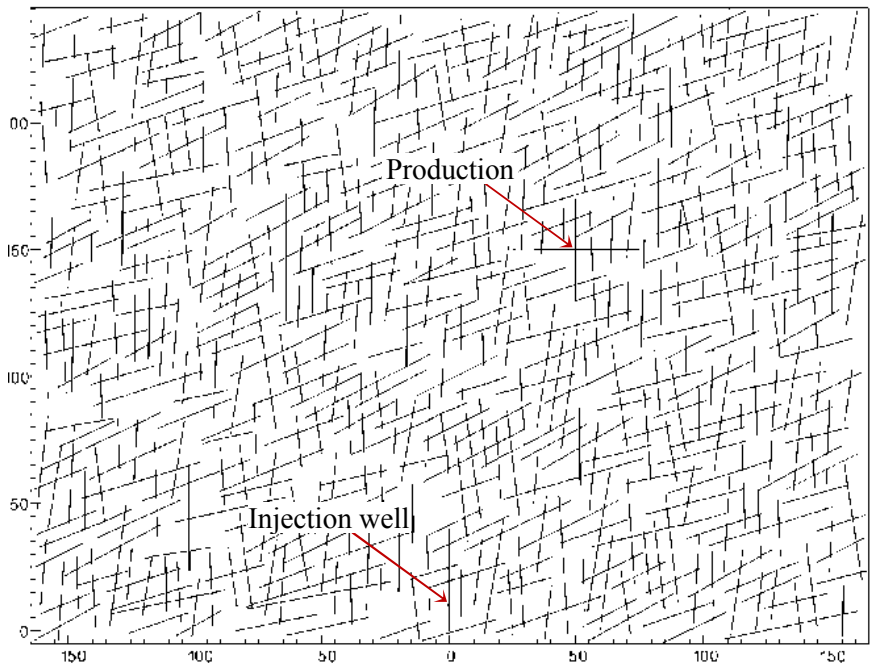

Figure 2 Layout of the naturally fractured reservoir.

In the baseline scenario, we inject fluid into the injection well at a constant pressure of 19.5 MPa, which is slightly lower than the minimum compressive principal stress to ensure that no fracture will be completely opened and invalidate the hydro-shearing regime assumption. Figure 3 shows the pressurized portion of the natural fracture network 5,000 and 20,000 seconds after the stimulation.

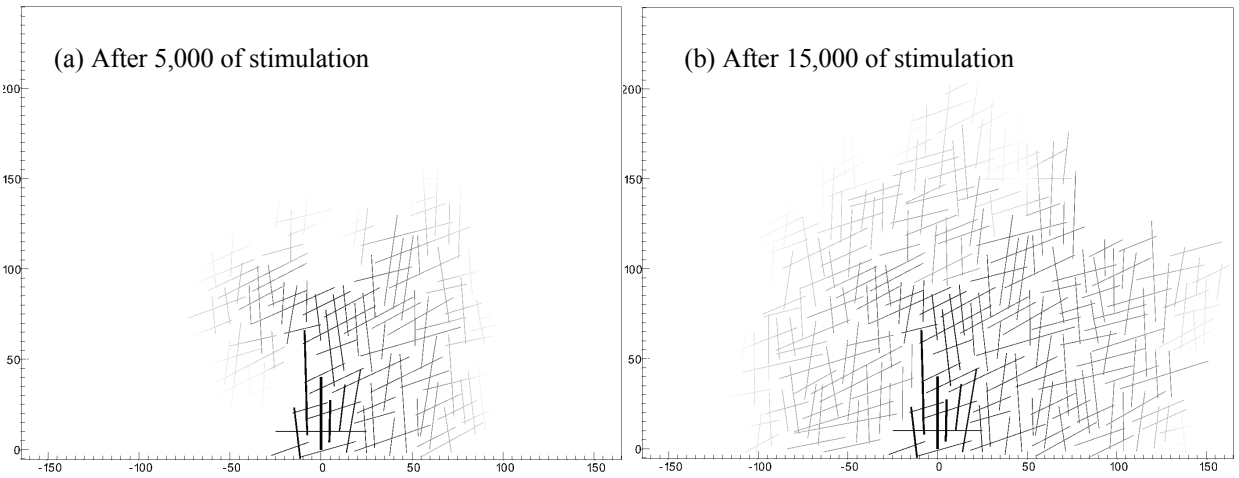

Figure 3 Pressurized fractures 5,000 seconds and 15,000 seconds after the stimulation starts in the baseline scenario. The darkness of the lines representing fractures illustrates the pressure, with black being the injection pressure and while being zero pressure (dry fracture).

In the second stimulation strategy evaluated here, while we inject through the injection well, we also inject at the same pressure (19.5 MPa) into the production well. 8,000 seconds after the simultaneous stimulation, we reduce the pressure at the production well to zero and fluid starts to flow out of this well from the reservoir. We term this stimulation strategy as the "*production well stimulation*" strategy. During the production phase, the region around the production well has the lowest fluid pressure, so the fractures connected to the production well are tightly closed, resulting in low local permeability. The production well stimulation strategy aims at improve the permeability near the production well through hydro-shearing, thereby increasing the flow rate into the production well and enhancing the fluid recovery ratio.

The distributions of the stimulation factor *S* along the natural fractures for these two stimulation scenarios are shown in Figure 4. In the baseline scenario, only a few fractures near the injection well are significantly stimulated with permanent permeability enhancement. In the second scenario, many more fractures between the two wells are stimulated, which is expected to result in enhanced permeability between them. In both scenarios only the vertical fracture set is stimulated, due to the high normal stress acting on the horizontal set. Meanwhile, although the horizontal fractures are also pressurized, the effective normal stress is not sufficiently reduced to allow shear dilation to take place. It should be noted that the vertical fractures alone cannot form flow channels between the two wells and horizontal fractures intersecting these vertical fractures must be involved. Nevertheless, the permeability enhancement to one set should result in significant permeability improvement of the overall fracture network. As shown in Figure 5, the flow rate into the production well for the second scenario is significantly higher than that of the baseline case, especially the flow though the upper branch.

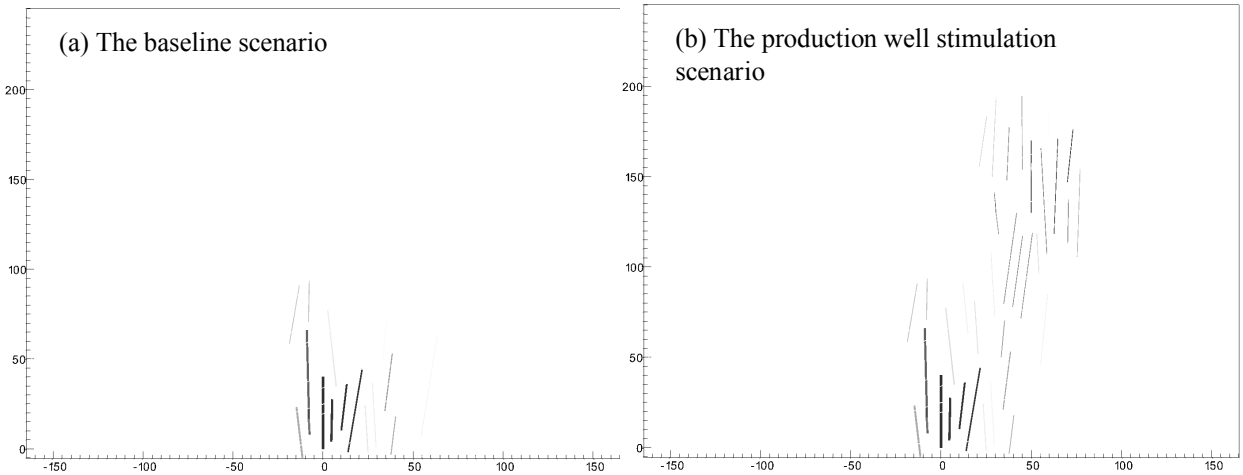

Figure 4 Distribution of the stimulation factor S along the natural fractures for the two stimulation scenarios. The darkness of fracture is mapped to the value of S, with black being S=2.0 and white (merged in background) being S=1.0. These are snapshots at 40,000 seconds after the stimulation has started.

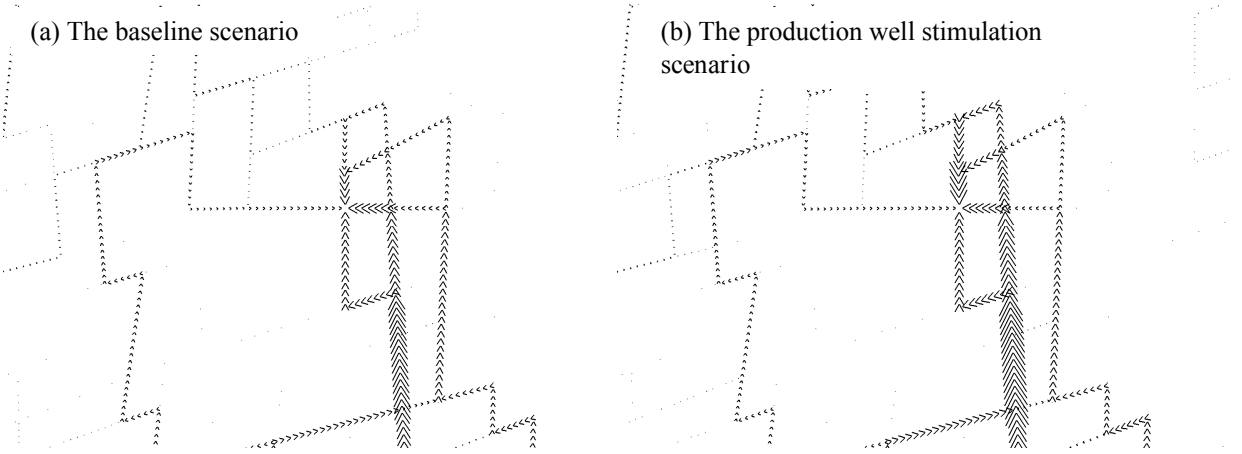

Figure 5 Flow rate near the production well at 40,000 seconds. The direction and size of the arrow heads represent the flow direction and flow rate, respectively.

Figure 6 tracks the flow rate at the two wells for both stimulation scenarios. In the production well stimulation scenario, the pressurized zone centered at the injection well and that originating from the production well significantly overlap and affect each other. Consequently, the injection into the production well reduces the absolute flow rate into the injection well during the stimulation. However, in the production phase when water is withdrawn from the production well, the injection rate for this scenario becomes slightly higher than that for the baseline scenario. At 16 hours after stimulation, the production well stimulation strategy increases the flow rates at the injection well and production well by 6% and 22%, respectively. It also enhances the fluid recovery ratio from 80% to 92%. Note that at 16 hours, the pressure front has just arrived at the boundaries of the simulation domain but it is not strictly speaking a steady state of the flow network. To simulate the reservoir responses beyond this state, a more realistic time-dependent flow boundary condition must be used, which is currently being researched. Nevertheless, the effects of the stimulation should remain the same during the long term production, at least in a qualitative and comparative sense.

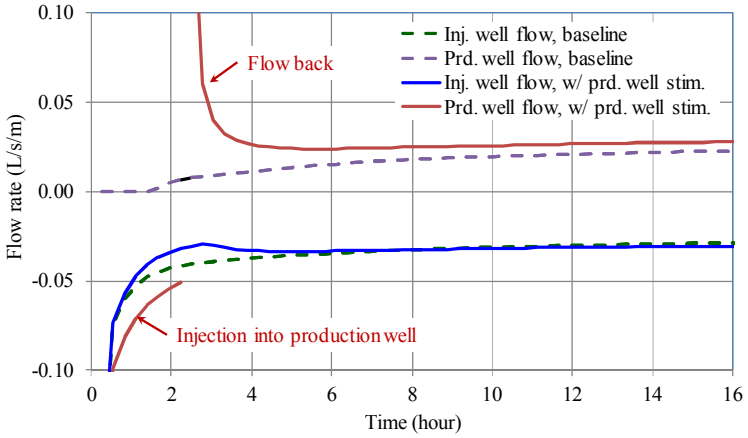

Figure 6 Flow rate into (negative value) and out of (positive value) the production well and the injection well for the two stimulation scenarios. Note that the flow rate at the beginning of the stimulation and the production well flow when flow-back just started is off the chart.

3. Concluding Remarks

In this study, we develop a discrete fracture network-based numerical model for the stimulation of naturally fractured reservoirs with hydraulic-shearing. We found that many physical processes, especially those related to interactions between neighbor pressurized fractures are fundamentally different from those in hydraulic fracturing. The new model for hydro-shearing is significantly different from and simpler than the fully coupled hydro-fracturing model that we developed earlier in Fu et al. (2011). We also used the new model to study the responses of a reservoir to two different stimulation scenarios in this paper. The new hydro-shearing model and the original hydro-fracturing model are complementary to each other. If applied jointed, it is possible to study hybrid stimulation scenarios involving both hydro-fracturing and hydro-shearing.

Auspices and Acknowledgements

The authors gratefully acknowledge the Geothermal Technologies Program of the US Department of Energy for support of this work under the Enhanced Geothermal Systems Program. The authors also would like to acknowledge their collaborators at the Lawrence Livermore National Laboratory. Additional support provided by the LLNL LDRD project "Creating Optimal Fracture Networks" (#11-SI-006) is gratefully acknowledged. This work was performed under the auspices of the U.S. Department of Energy by Lawrence Livermore National Laboratory under Contract DE-AC52-07NA27344. This document is LLNL report LLNL-CONF-554011.

REFERENCES

MIT, 2006. The Future of Geothermal Energy: Impact of Enhanced Geothermal Systems (EGS) on the United States in the 21st Century.

Willis-Richards J., Watanabe K., and Takahashi H, 1996. "Progress toward a stochastic rock mechanics model of engineered geothermal systems." *Journal of Geophysical Research*, 101(B8): 17481–17496.

Jing Z., Willis-Richards J., Watanabe K., and Hashida T., 2000. "A three-dimensional stochastic rock mechanics model of engineered geothermal systems in fractured crystalline rock." *Journal of Geophysical Research*, 105(B10): 23663–23679.

Rahman M.K., Hossain M.M., and Rahman S.S., 2002. "A shear-dilation-based model for evaluation of hydraulically stimulated naturally fractured reservoirs." *International Journal for Numerical and Analytical Methods in Geomechanics*, 26(5): 469-497.

Tezuka K., Tamagawa T., and Watanabe K., 2005. "Numerical simulation of hydraulic shearing in fractured reservoir." *Proceedings of World Geothermal Congress*, Antalya, Turkey.

Cladouhos T.T., Clyne, ., Osborn, W.L., Nichols, M., Petty, S., and Nofziger, Laura., 2011. "Newberry volcano EGS demonstration stimulation modeling." Proceedings of the 35th Annual Meeting of Geothermal Resources Council, San Diego, CA.

Barton, N., Bandis, S., Bakhtar, K. (1985), "Strength, deformation and conductivity coupling of rock joints," *International Journal of Rock Mechanics and Mining Sciences & Geomechanics Abstracts*, 22(3), 121-140.

Bandis, S., Lumsden, A., Barton, N. (1983), "Fundamentals of rock joint deformation," *International Journal of Rock Mechanics and Mining Sciences & Geomechanics Abstracts*, 20(6), 249-268.

Fu, P., Johnson, S.M., Hao, Y., and Carrigan, C.R. (2011), "Fully coupled geomechanics and discrete flow network modeling of hydraulic fracturing for geothermal applications." *The 36th Stanford Geothermal Workshop*, Jan. 31 – Feb. 2, 2011, Stanford, CA.